Electronic Supplementary Material (ESI) for ChemComm.
This journal is © The Royal Society of Chemistry 2015

Electronic supplementary information (ESI) for

Separating mixtures of polar compounds using a flexible metal-organic framework

Radha Kishan Motkuri,[†] Praveen K. Thallapally, *[‡] Harsha. V. R. Annapureddy,[‡] Liem Dang,[‡] Rajamani Krishna,*[Π] Satish K Nune,[†] Carlos. A. Fernandez, Jian Liu,[†] B. Peter McGrail,[†]*

[†] Energy and Environment Directorate, Pacific Northwest National Laboratory, Richland, WA 99352, USA.

[‡] Fundamental and Computational Sciences Directorate, Pacific Northwest National Laboratory, Richland, WA 99352, USA.

[Π] Van ‘t Hoff Institute for Molecular Sciences, University of Amsterdam,
Science Park 904, 1098 XH Amsterdam, The Netherlands

*To whom correspondence: Radhakishan.Motkuri@pnnl.gov; praveen.thallapally@pnnl.gov; R.Krishna@contact.uva.nl

Table of Contents

Section S1: Materials and Methods

Experimental Procedure:

TetZB (Scheme 1): The flexible tetrahedral organic linker **1** was successfully synthesized using a reported procedure, and further synthesis of TetZB MOF was reported by us previously.[1] Briefly, a solid mixture of flexible linker **1** (0.06 g, 0.1mmol, 1 equiv), bipyridine (0.015 g, 0.1mmol, 1 equiv, Aldrich), and $Zn(NO_3)_2 \cdot 6H_2O$ (0.03 g, 0.1 mmol, 1 equiv, Aldrich) was dissolved in 10 mL DMF in a 20 mL vial. The reaction mixture was mixed thoroughly and ultrasonicated until it became clear. The reaction vial was capped tightly and placed in an oven at 100 °C. After 24 hours, the sample was removed from the oven and allowed to cool to room temperature (RT). The mother liquor was decanted to obtain transparent crystals that then were washed with DMF (3 mL × 3) and dried in air for 10 min.

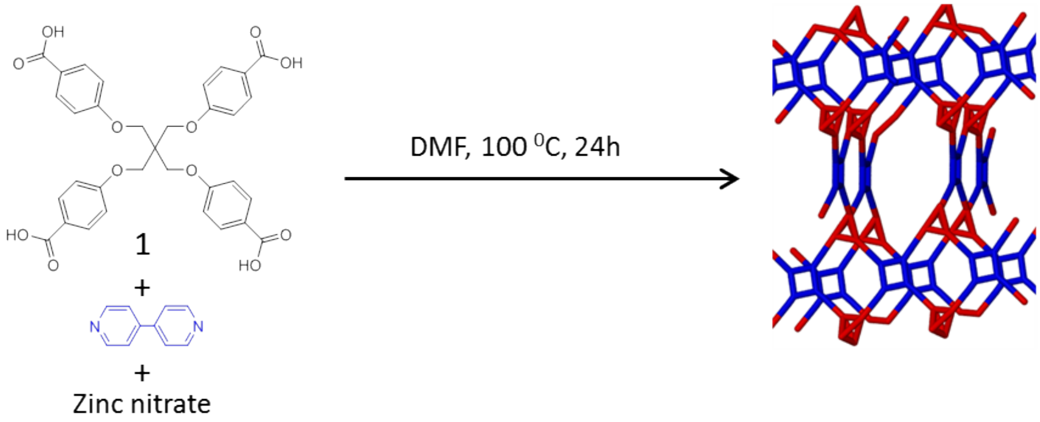

Scheme S1

Section S2. Sorption isotherms of various polar solvents in TetZB:

Prior to measuring adsorption, the TetZB sample was placed in a container of the IGA chamber and the weight of the sample was recorded before activation. The temperature of the furnace was increased up to 250°C under vacuum at a rate of 5°C/min to remove the trapped solvent molecules. The sample was cooled to RT, its dry mass was set, and the experimental temperature 25°C was maintained by the IGA water bath. The static mode of the IGA was used to measure the sorption of polar solvents isothems. The pressure points were set beforehand using the IGA software. The pressure was maintained at the set point by active computer control of the inlet/outlet valves throughout the duration of the experiment. Weight increases resulting from adsorption at each pressure step were plotted against the pressure.

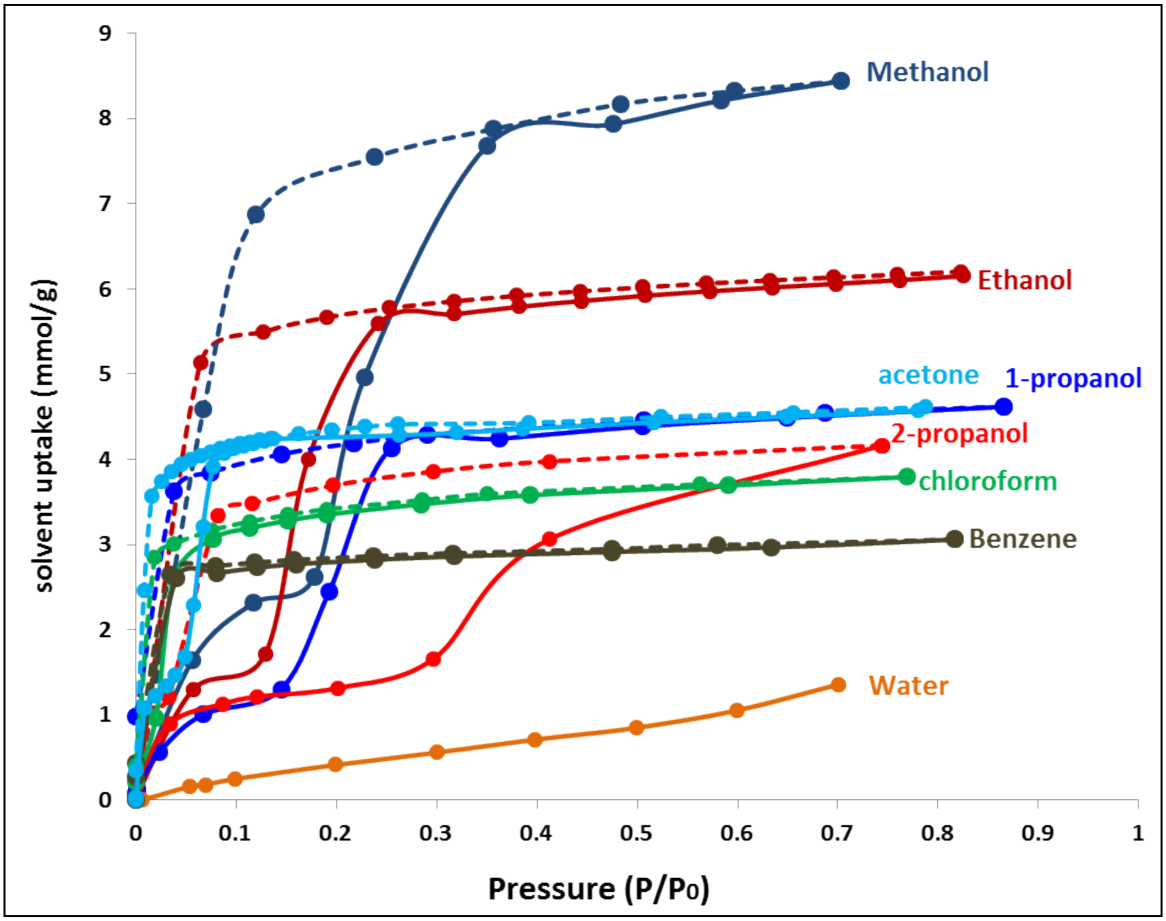

Figure S1: Reversible adsorption and desorption (mmol/g) isotherms of various polar solvents in TetZB at 25°C.

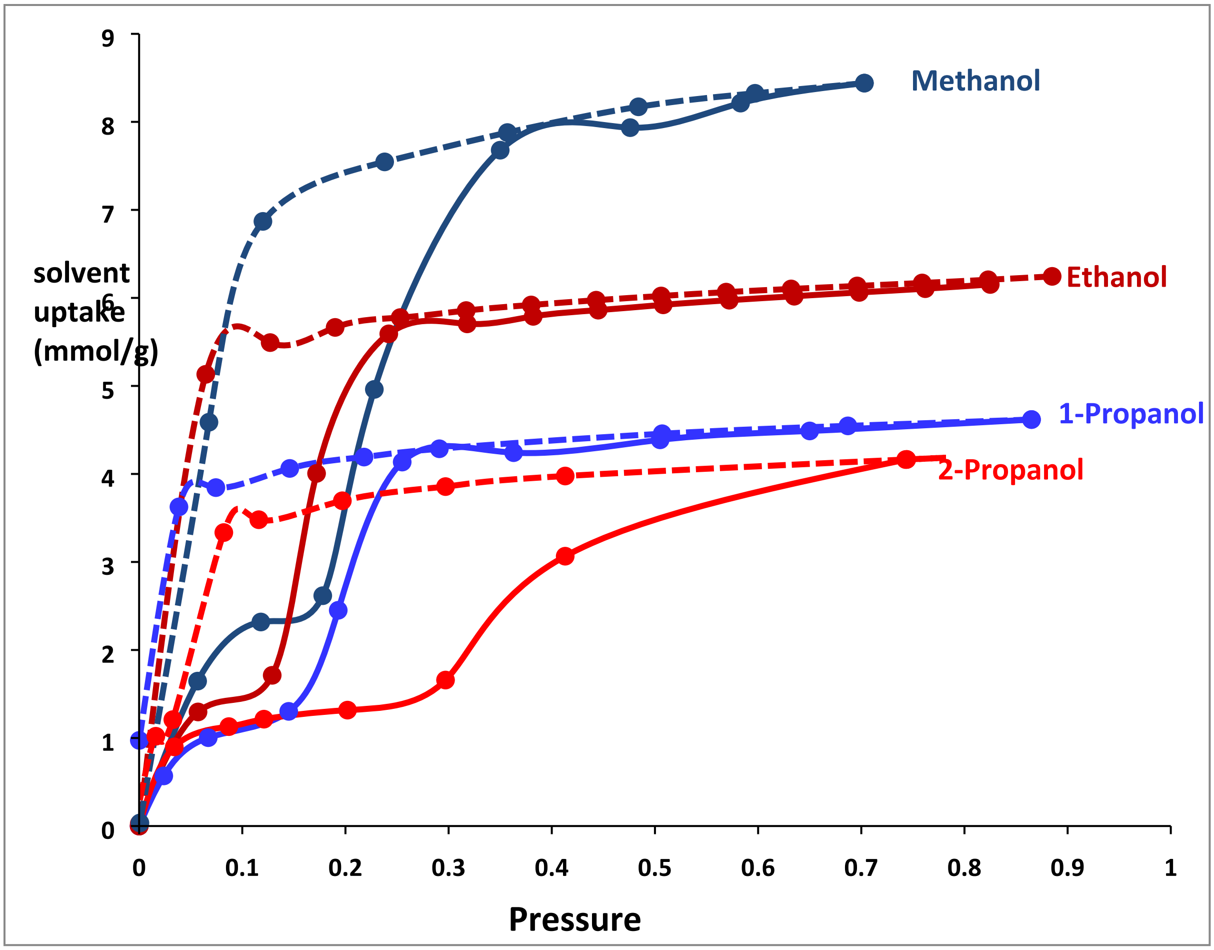

Figure S2: Reversible adsorption and desorption in mmol/g of C1–C3 alcohols at RT.

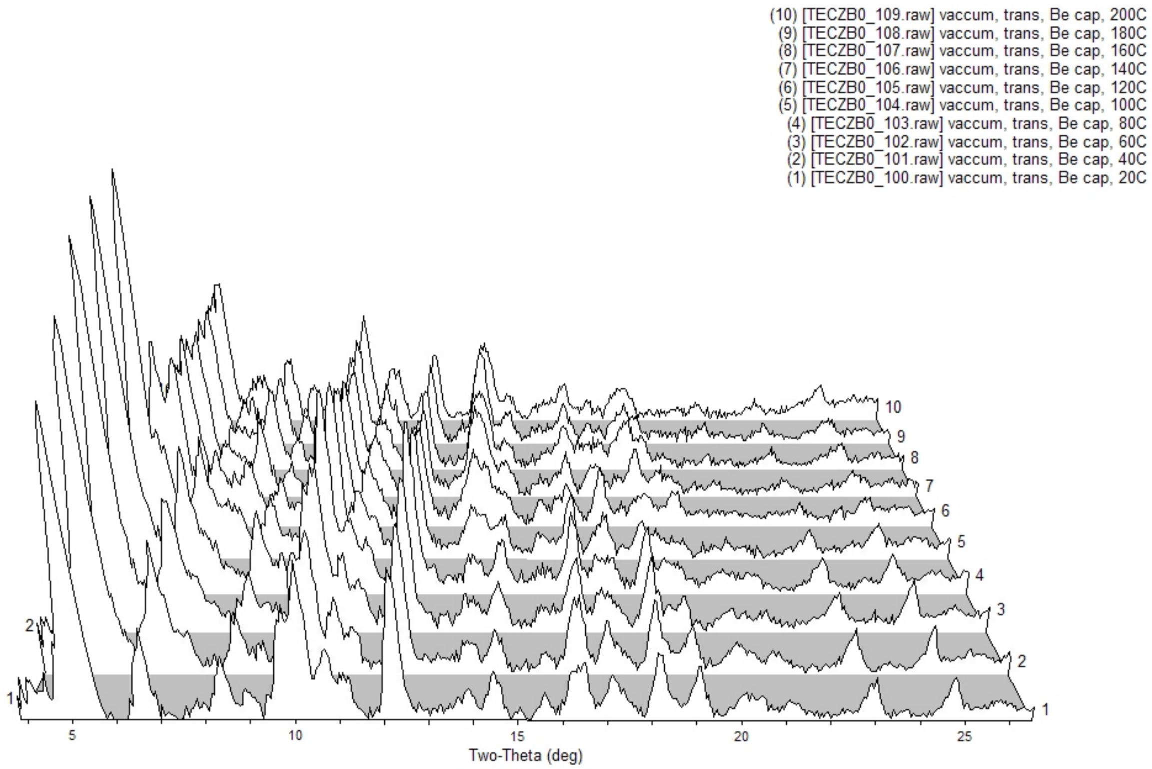

Figure S3: Powder XRD of the sample TetZB from 25°C to 200°C. Note the change in structure at 140°C.

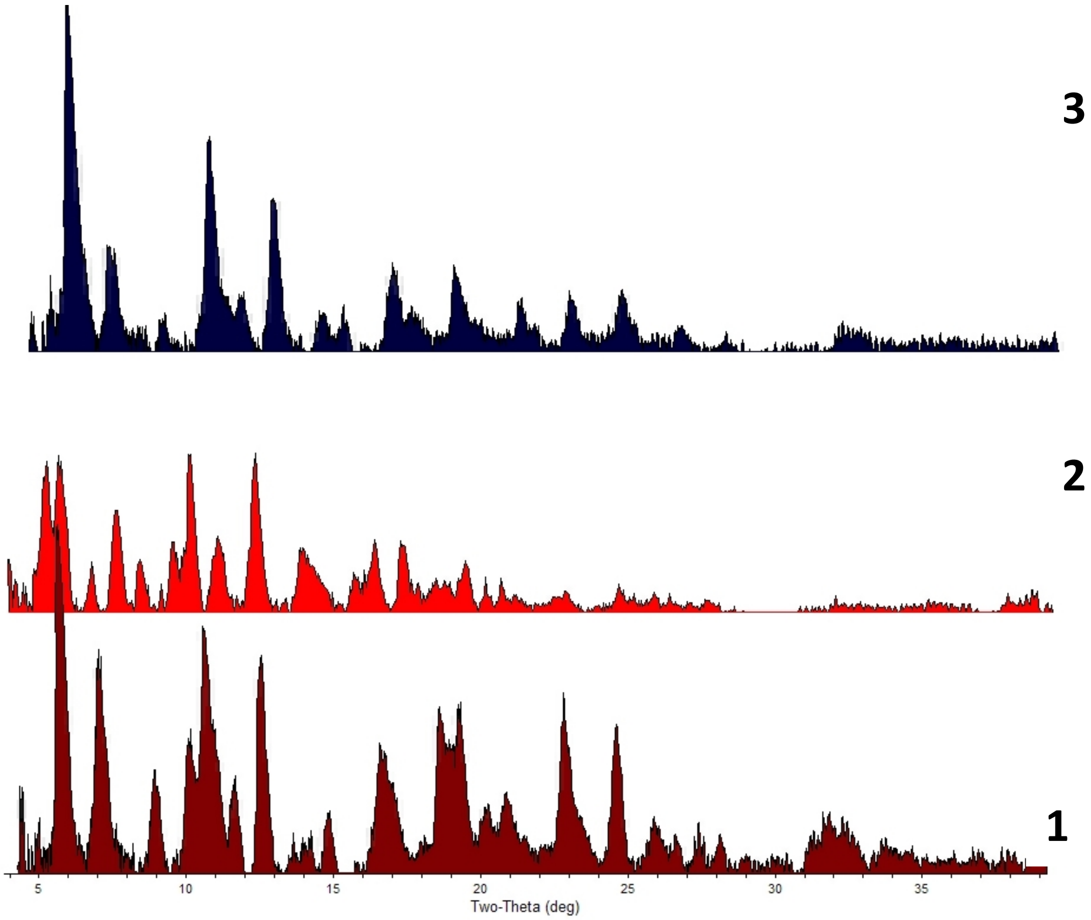

Figure S4. Powder XRD spectra of TetZB at (1) RT, (2) heated at 200°C under vacuum, and (3) exposed to methanol vapors for 24 hours.

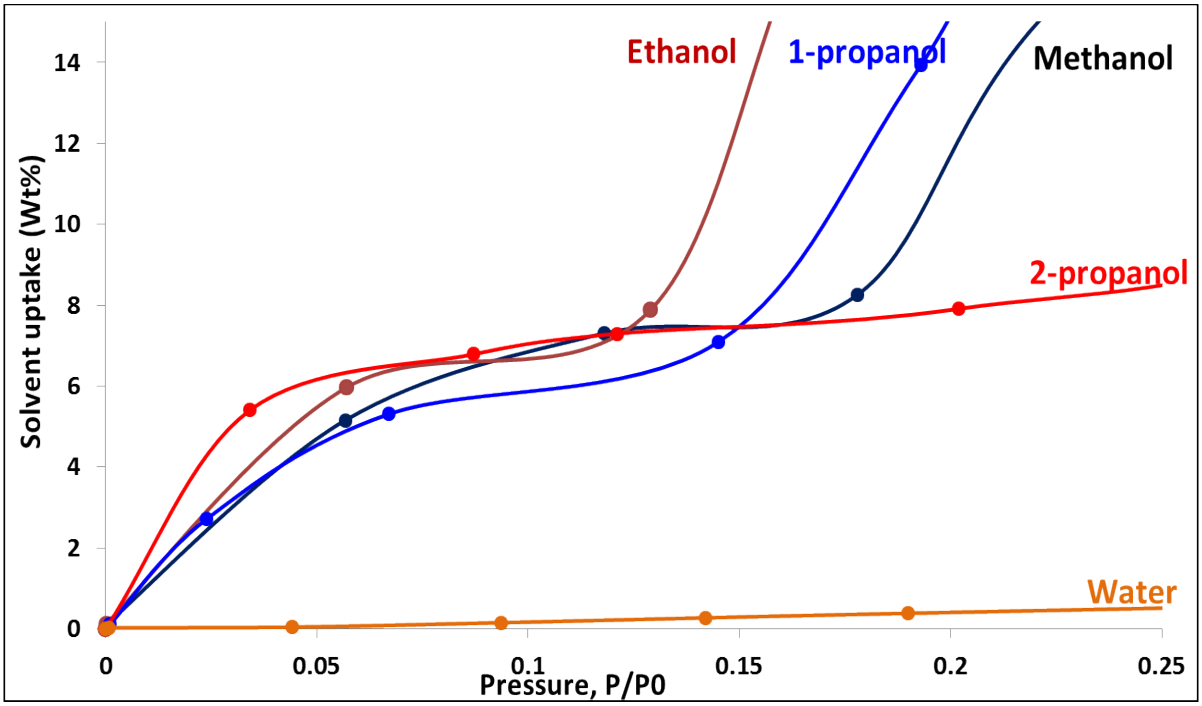

Figure S5: The expanded low partial pressure region of alcohols sorption isotherms in TetZB at 298K.

Table S1: Fundamental properties of adsorbents and their experimental sorption capacities in activated TetZB at 298K. Sorption capacities in wt% and corresponding values in mmol/g are provided for clarity. The dipole moments were taken from the reference Kitagawa et al 2011.[2]

Adsorbents	Structure	Kinetic diameter (Å)	Dipole moment (D)	Experimental Uptake wt% (mmol/g)
Methanol	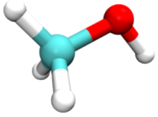	3.6-4.0	1.69	27.0 (8.44)
Ethanol	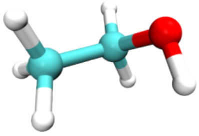	4.3-4.5	1.71	28.3(6.15)
1-propanol	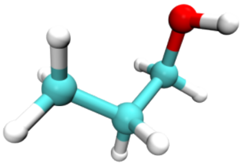	4.7	1.49	27.7 (4.6)
2-propanol	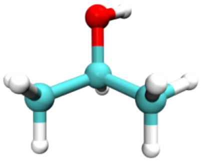	4.7	1.56	25.0 (4.16)
Water	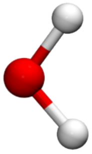	2.6-2.9	1.86	2.44 (1.35)

Section S3: Grand Canonical Monte Carlo (GCMC) Modeling Studies:

To increase computational efficiency, the TetZB structure and the guest molecules are assumed to be rigid. Intermolecular interactions between the MOF framework and guest molecules were described by Lennard-Jones (LJ) and electrostatic interactions. GCMC simulations were performed with four types of moves: 1) molecular displacement, 2) molecular rotation, 3) insertion of a molecule with random orientation into a random position in the system, and 4) deletion of a randomly chosen molecule from the system. At each pressure point, we performed 2×10^7 trial moves for GCMC simulations. Because the host framework considered has a rigid structure, the breathing phenomenon was not observed; however, the overall uptake of the solvents matched the experimental results at 25°C. In the case of propanol isomers, both simulations and experiments show that the adsorption isotherm for 2-propanol was steeper at lower loadings compared to 1-propanol. To understand this behavior, we computed the interaction energies between MOF and propanol isomers as a function of loading. We obtained more negative interaction energies for 2-propanol compared to 1-propanol, which clearly indicates stronger a interaction between TetZB and 2-propanol at lower loadings, but overall, the observed loading for 1-propanol was slightly higher.

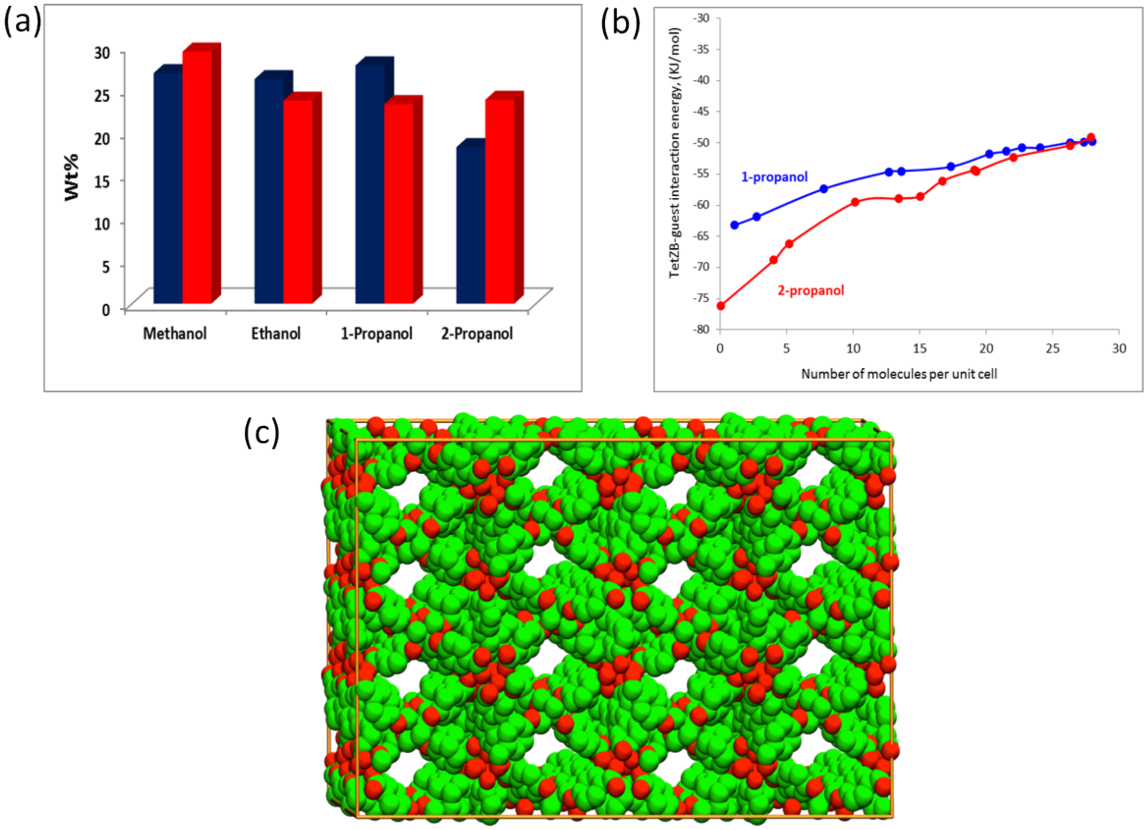

Figure S6: (a) Comparison of experimental (blue) vs. modeling (red) sorption studies of solvents in TetZB at P/P_0=0.7; (b) TetZB-guest 1-/2-propanol interaction energy calculations at lower loadings; (c) TetZB structure showing aromatic hydrophobic (green) and metallic (hydrophilic-red) in CPK model.

Section S4: Fitting of Isotherms:

The experimentally measured loadings of water, methanol, ethanol, 1-propanol, 2-propanol, acetone, benzene, and chloroform in TetZB obtained at RT (i.e., 298 K) were fitted with the dual-site Langmuir-Freundlich model.

$$q = q_{A,sat} \frac{b_A p^{\nu_A}}{1 + b_A p^{\nu_A}} + q_{B,sat} \frac{b_B p^{\nu_B}}{1 + b_B p^{\nu_B}} \tag{1}$$

The Langmuir-Freundlich parameters are provided in Table S2. Figure S4 provides a comparison of the pure component isotherm data with dual-site Langmuir-Freundlich fits. The isotherms of all guest adsorbates water, methanol, ethanol, 1-propanol, 2-propanol, acetone, benzene and chloroform exhibit steep increases. Such steep increases are traceable to molecular clustering effects induced by hydrogen bonding; this has been established in the publications of Krishna and van Baten.[3] To properly capture the steep isotherms, the Freundlich exponent needs to have large values in the range of 5 to 10.

The pure component isotherm data for water extends only to $p/p_0 = 0.95$ at which the saturation capacity is not reached. Consequently, the uncertainties for isotherm fits for water are significant. Nevertheless, the calculations presented below for adsorption equilibrium, and breakthroughs are expected to be of reasonable accuracy.

Section S5: Simulation Methodology for Transient Breakthrough in Fixed-Bed Adsorbers

Fixed bed adsorbers packed with crystals of microporous materials are commonly used for separation of mixtures; such adsorbers are commonly operated in a transient mode, and the compositions of the gas phase and the component loadings within the crystals vary with position and time. During the initial stages of the transience, the pores are loaded gradually, and only towards the end of the adsorption cycle are conditions corresponding to pore saturation achieved. In other words, separations in a fixed bed adsorber are influenced by both the Henry regime of adsorption as well as the conditions corresponding to pore saturation. Experimental data on the transient breakthrough of mixtures across fixed beds are commonly used to evaluate and compare the separation performance of zeolites and MOFs.[4] For a given separation task, transient breakthroughs provide more a realistic evaluation of the efficacy of a material, as they reflect the combined influence of adsorption selectivity, adsorption capacity, and intra-crystalline diffusion limitations.[4e, 5]

We describe below the simulation methodology used to perform transient breakthrough calculations that are presented in this work. This simulation methodology is the same as that used in our previously published work.[4e]

Assuming plug flow of an n-component gas mixture through a fixed bed maintained under isothermal conditions, the partial pressures in the gas phase at any position and instant of time are obtained by solving the following set of partial differential equations for each of the species *i* in the gas mixture.[6]

$$\frac{1}{RT}\frac{\partial p_i(t,z)}{\partial t} = -\frac{1}{RT}\frac{\partial\left(v(t,z)p_i(t,z)\right)}{\partial z} - \frac{(1-\varepsilon)}{\varepsilon}\rho\frac{\partial \overline{q}_i(t,z)}{\partial t}; \quad i = 1,2,...n \tag{2}$$

In equation (2), t is the time, z is the distance along the adsorber, ρ is the framework density, ε is the bed void volume, v is the interstitial gas velocity, and $\overline{q}_i(t,z)$ is the *spatially averaged* molar loading within the crystallites of radius r_c, monitored at position z, and at time t.

At any time t, during the transient approach to thermodynamic equilibrium, the spatially averaged molar loading within the crystallite r_c is obtained by integration of the radial loading profile.

$$\overline{q}_i(t) = \frac{3}{r_c^3}\int_0^{r_c} q_i(r,t)r^2 dr \tag{3}$$

For transient unary uptake within a crystal at any position and time with the fixed bed, the radial distribution of molar loadings, q_i, within a spherical crystallite, of radius r_c, is obtained from a solution of a set of differential equations describing the uptake

$$\frac{\partial q_i(r,t)}{\partial t} = -\frac{1}{\rho}\frac{1}{r^2}\frac{\partial}{\partial r}\left(r^2 N_i\right) \tag{4}$$

The molar flux N_i of component i is described by the simplified version of the Maxwell-Stefan equations in which both correlation effects and thermodynamic coupling effects are considered to be of negligible importance.[4e]

$$N_i = -\rho Đ_i \frac{\partial q_i}{\partial r} \tag{5}$$

Summing equation (**3**) over all n species in the mixture allows calculation of the *total average* molar loading of the mixture within the crystallite.

$$\overline{q}_t(t,z) = \sum_{i=1}^{n}\overline{q}_i(t,z) \tag{6}$$

The *interstitial* gas velocity is related to the *superficial* gas velocity by equation (7).

$$v = \frac{u}{\varepsilon} \tag{7}$$

In industrial practice, the most common operation is to use a step-wise input of mixtures to be separated into an adsorber bed that is initially free of adsorbates; that is, with the initial condition described by equation (8).

$$t = 0; \quad q_i(0, z) = 0 \tag{8}$$

At time, $t = 0$, the inlet to the adsorber, $z = 0$, is subjected to a step input of the n-component gas mixture, and this step input is maintained until the end of the adsorption cycle when steady-state conditions are reached.

$$t \geq 0; \quad p_i(0,t) = p_{i0}; \quad u(0,t) = u \tag{9}$$

where u is the superficial gas velocity at the inlet to the adsorber.

If the value of $\frac{Đ_i}{r_c^2}$ is large enough to ensure that intra-crystalline gradients are absent and the entire crystallite particle can be considered to be in thermodynamic equilibrium with the surrounding bulk gas phase at that time t, and position z of the adsorber

$$\overline{q}_i(t, z) = q_i(t, z) \tag{10}$$

The molar loadings at the *outer surface* of the crystallites (i.e., at $r = r_c$,) are calculated on the basis of adsorption equilibrium with the bulk gas phase partial pressures p_i at that position z and time t. The adsorption equilibrium can be calculated on the basis of the Ideal Adsorbed Solution Theory (IAST) of Myers and Prausnitz.[7]

For presenting the breakthrough simulation results, we use the dimensionless time, $\tau = \frac{tu}{L\varepsilon}$, obtained by dividing the actual time, t, by the characteristic time, $\frac{L\varepsilon}{u}$, where L is the length of adsorber, u is the superficial fluid velocity, ε is the bed voidage.[5] For all the simulations reported in this article, we choose $L = 0.3$ m; $u = 0.04$ m s^{-1}; $\varepsilon = 0.4$.

Table S2: Dual-site Langmuir-Freundlich parameters for adsorption of water, methanol, ethanol, 1-propanol, 2-propanol, chloroform, benzene, and acetone at 298 K in TetZB. These fits are for the “adsorption” branch of the isotherms.

Adsorbate	Site A			Site B		
	$q_{\mathrm{A,sat}}$ mol kg^{-1}	b_{A0} $\mathrm{Pa}^{-\nu_A}$	$\square_{\mathrm{A}}$ dimensionless	$q_{\mathrm{B,sat}}$ mol kg^{-1}	b_{B0} $\mathrm{Pa}^{-\nu_B}$	$\square_{\mathrm{B}}$ dimensionless
Water	3	4.01×10^{-5}	0.94	18	3.02×10^{-46}	13
Methanol	4.6	1.28×10^{-36}	10	6	5.08×10^{-3}	0.62
Ethanol	3.6	3.97×10^{-38}	12	3.2	8.4×10^{-3}	0.7
1-propanol	2.7	5.92×10^{-35}	12.5	2.5	2.79×10^{-2}	0.6
2-propanol	2.7	4.83×10^{-27}	7.8	1.7	4.43×10^{-2}	0.6
Chloroform	1.75	1.22×10^{-39}	13.2	2.7	4.76×10^{-2}	0.4
Benzene	1.6	1×10^{-36}	17.5	17	2.97×10^{-2}	0.12
Acetone	3	6.48×10^{-14}	4	2.6	2.49×10^{-1}	0.2

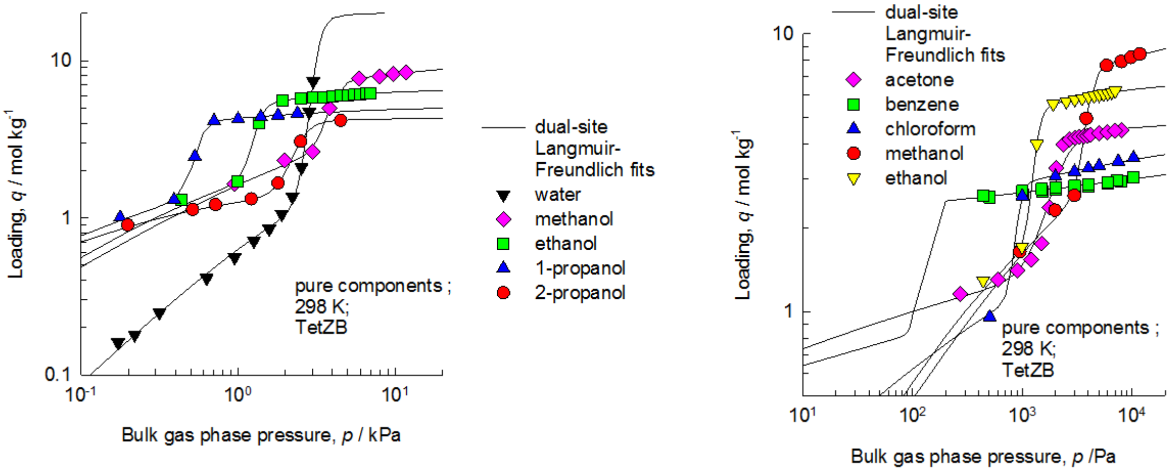

Figure S7. Comparison of the pure component isotherm data with dual-site Langmuir-Freundlich fits (parameters as provided in Table S2) or adsorption of water, methanol, ethanol, 1-propanol, 2-propanol, acetone, benzene, and chloroform in TetZB obtained at 298 K.

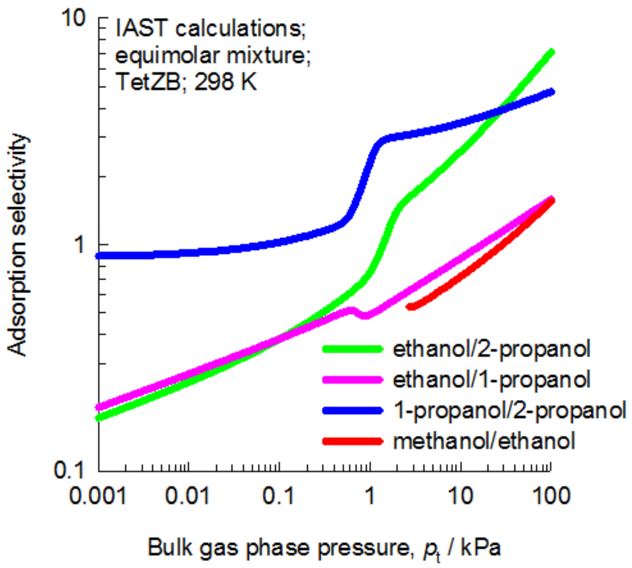

Figure S8. IAST calculations for binary adsorption equilibrium for equimolar methanol/ethanol, 1-propanol/2-propanol, ethanol/1-propanol, and ethanol/2-propanol in TetZB at 298 K.

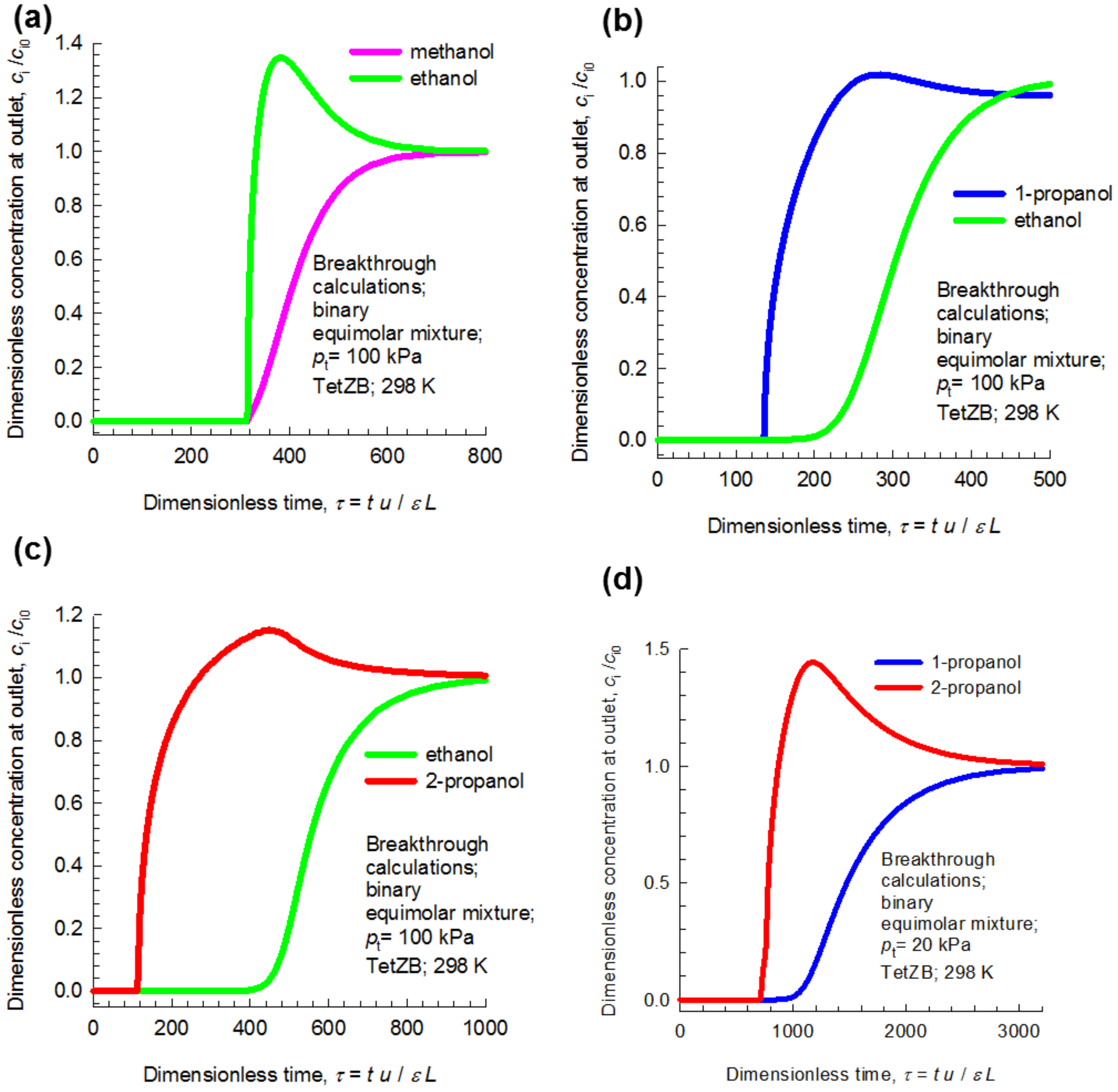

Figure S9. Transient breakthrough simulations for (a) 50/50 methanol/ethanol, (b) 50/50 ethanol/1-propanol, (c) 50/50 ethanol/2-propanol, and (d) 50/50 1-propanol/2-propanol mixture in a fixed-bed adsorber packed with TetZB at 298 K. In (a), (b), and (c), the total pressure is 100 kPa; in (d), the total pressure is 20 kPa. Intra-crystalline diffusion effects are accounted for by taking $Ð_{methanol}/r_c^2 = 2\times10^{-3}$ s^{-1}; $Ð_{ethanol}/r_c^2 = 1\times10^{-3}$ s^{-1}; $Ð_{1-proanol}/r_c^2 = Ð_{2-propanol}/r_c^2 = 1\times10^{-4}$ s^{-1}.

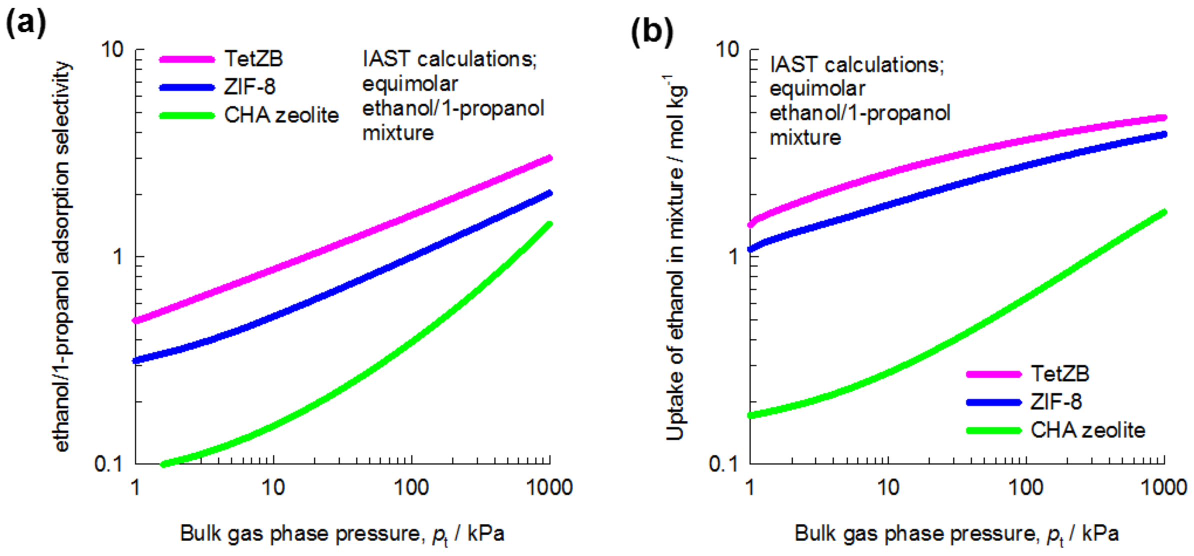

Figure S10. Comparison of (a) ethanol/1-propanol adsorption selectivity and (b) uptake capacity of ethanol for equimolar ethanol/1-propanol mixtures in TetZB, ZIF-8, and CHA zeolite. The comparisons are based on IAST calculations.

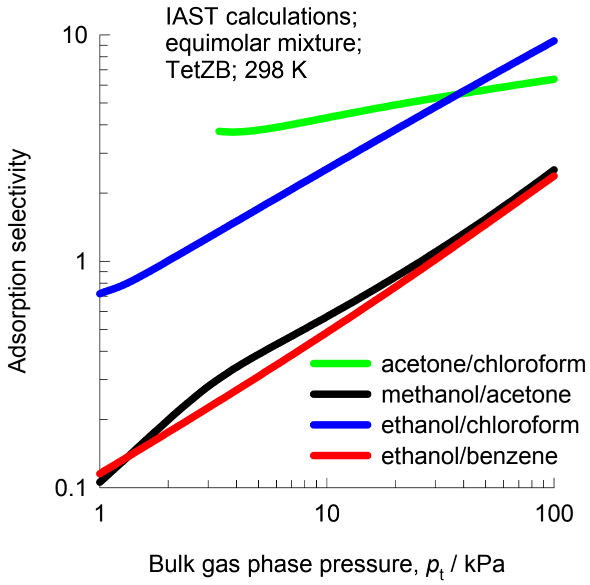

Figure S11. IAST calculations for binary adsorption equilibrium for equimolar acetone/chloroform, methanol/acetone, ethanol/chloroform, and ethanol/benzene at 298 K.

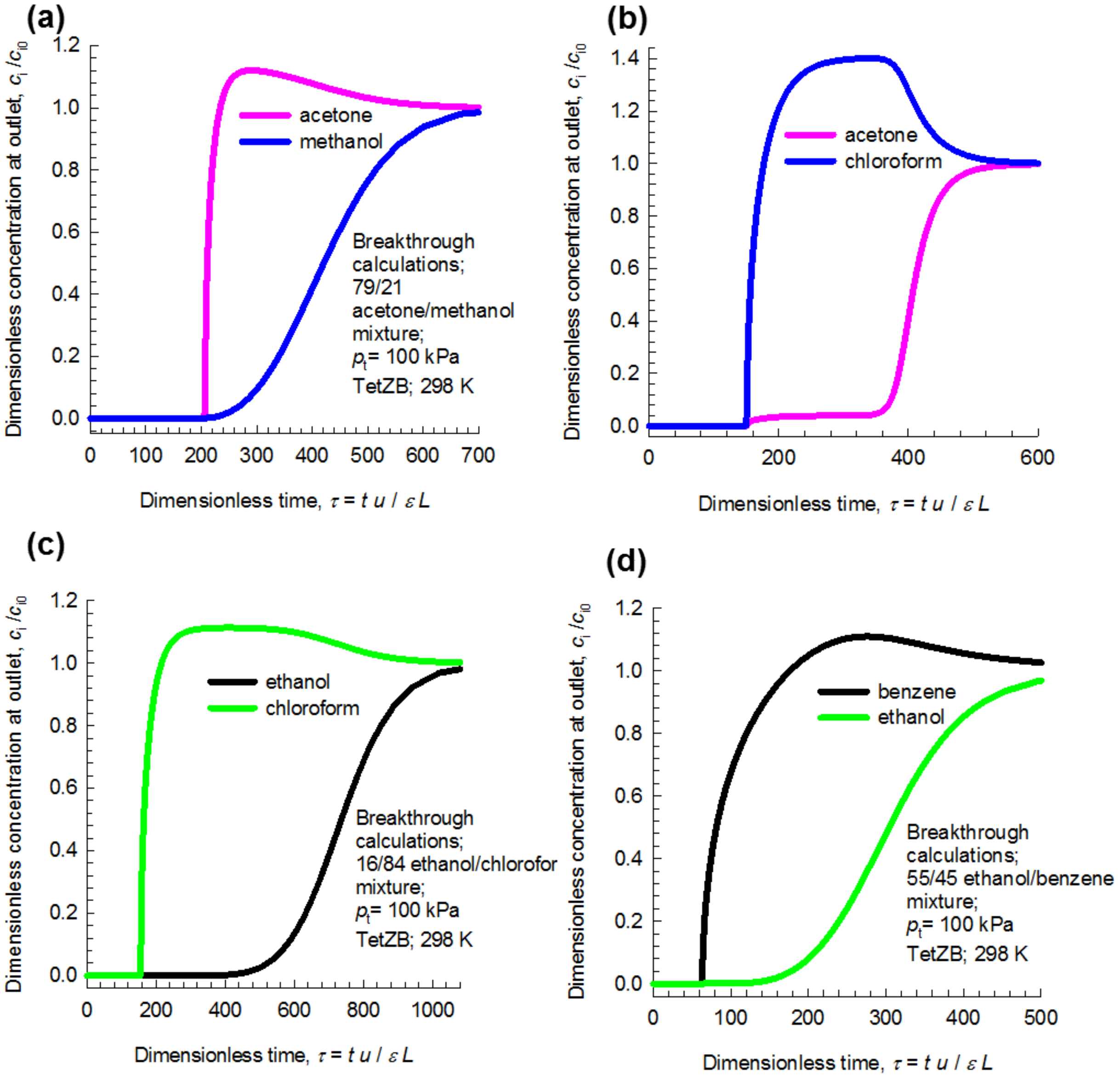

Figure S12. Transient breakthrough simulations for (a) 79/21 acetone/methanol, (b) 34/66 acetone/chloroform, (c) 16/84 ethanol/chloroform, and (d) 55/45 ethanol/benzene mixtures in a fixed-bed adsorber packed with TetZB at 298 K. The total pressure is 100 kPa. Intra-crystalline diffusion effects are accounted for by taking $Đ_{methanol}/r_c^2 = 2\times10^{-3}$ s^{-1}; $Đ_{ethanol}/r_c^2 = 1\times10^{-3}$ s^{-1}; $Đ_{acetone}/r_c^2 = 2\times10^{-3}$ s^{-1}; $Đ_{chloroform}/r_c^2 = 1\times10^{-3}$ s^{-1}; $Đ_{benzene}/r_c^2 = 1\times10^{-4}$ s^{-1}.

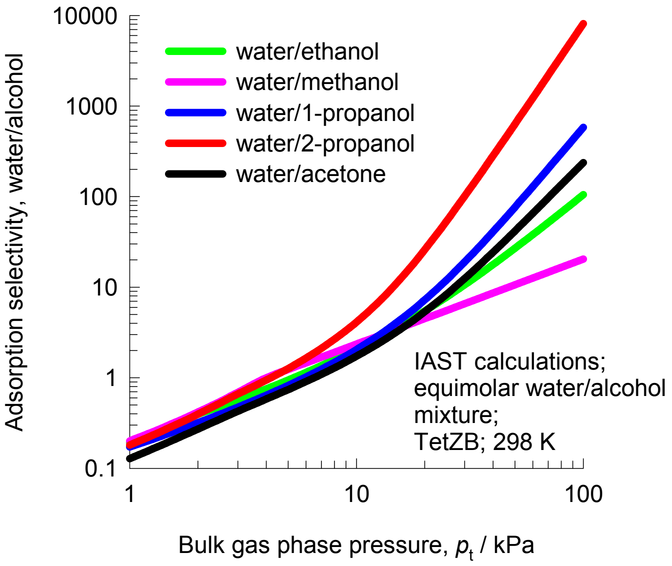

Figure S13: IAST calculations for binary adsorption equilibrium for equimolar water/methanol, water/ethanol, water/1-propanol, water/2-propanol, and water/acetone mixtures in TetZB at 298 K.

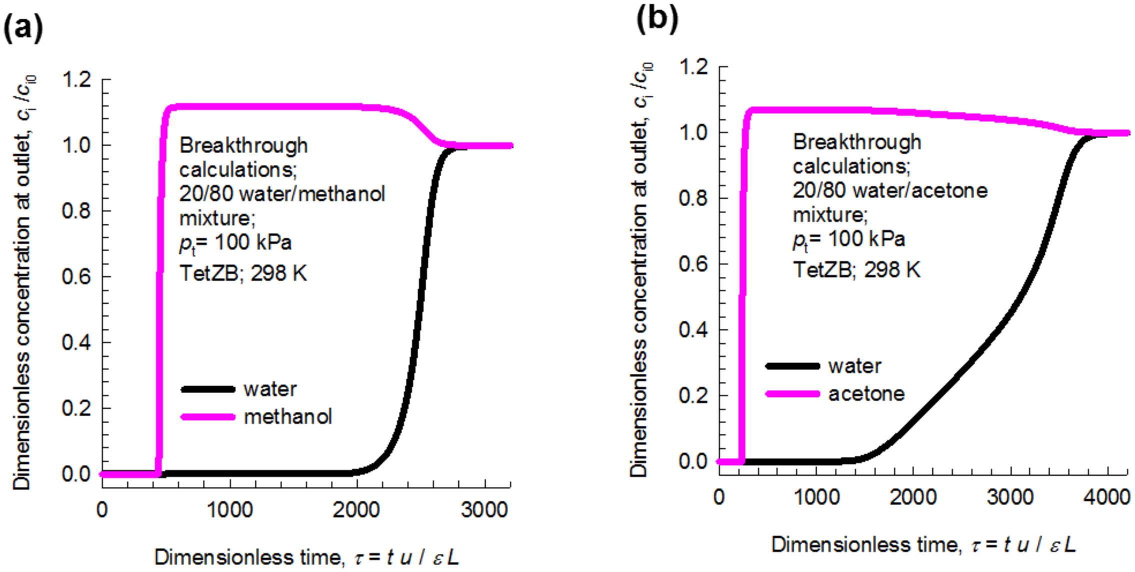

Figure S14: Transient breakthrough simulations for (a) 20/80 water/methanol, and (b) 20/80 water/acetone mixture in a fixed-bed adsorber packed with TetZB at 298 K. The total pressure is

100 kPa. Intra-crystalline diffusion effects are accounted for by taking $Đ_{water}/r_c^2 = 1\times10^{-3}\ \mathrm{s^{-1}}$; $Đ_{methanol}/r_c^2 = 2\times10^{-3}\ \mathrm{s^{-1}}$; $Đ_{acetone}/r_c^2 = 2\times10^{-3}\ \mathrm{s^{-1}}$.

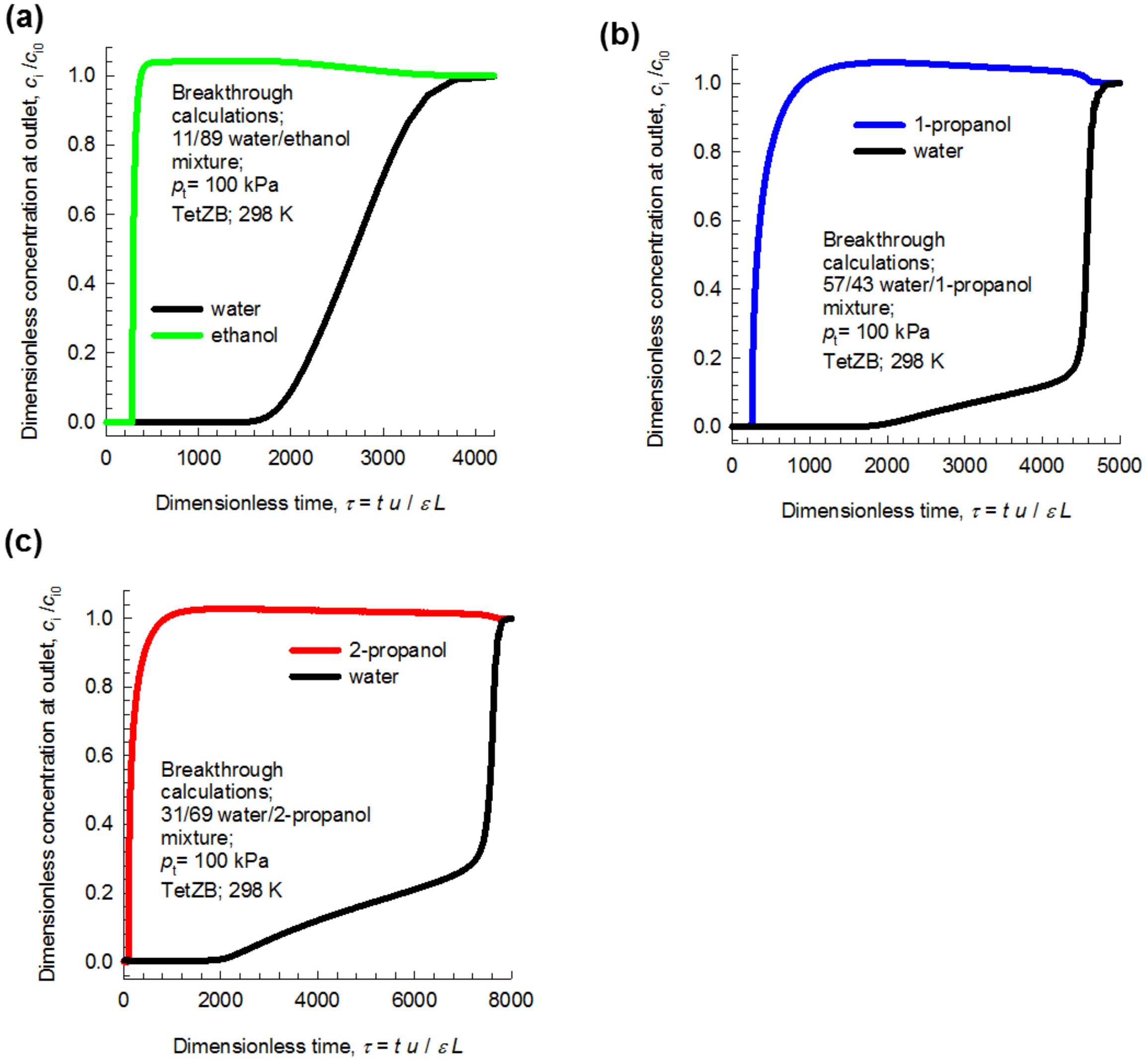

Figure S15: Transient breakthrough simulations for (a) 11/89 water/ethanol, (b) 57/43 water/1-propanol, and (c) 31/69 water/2-propanol mixture in a fixed-bed adsorber packed with TetZB at 298 K. The total pressure is 100 kPa. Intra-crystalline diffusion effects are accounted for by taking $Đ_{water}/r_c^2 = 1\times10^{-2}\ \mathrm{s^{-1}}$; $Đ_{ethanol}/r_c^2 = 1\times10^{-3}\ \mathrm{s^{-1}}$; $Đ_{1-proanol}/r_c^2 = 1\times10^{-4}\ \mathrm{s^{-1}}$; $Đ_{2-propanol}/r_c^2 = 1\times10^{-4}\ \mathrm{s^{-1}}$.

Section S6: Schematic of adsorber packed with TetZB

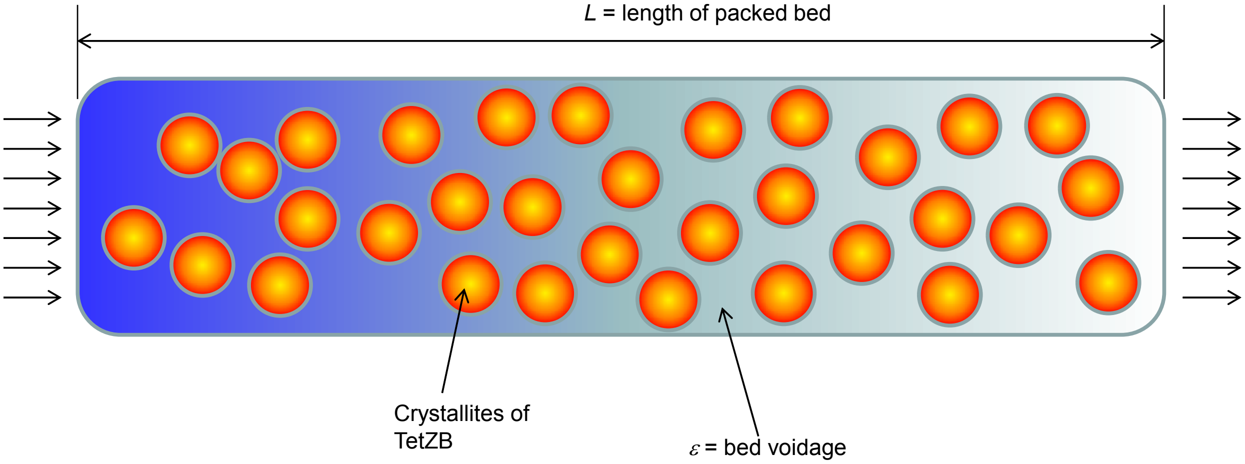

Figure S16: Schematic of adsorber packed with TetZB.

Section S7: Explanation on the Video Animations

In the transient breakthrough simulations, a binary vapor mixture, for example of 1-propanol/1-propanol is injected at time $t = 0$ at the inlet to the fixed bed packed with crystallites of TetZB.

The video animations, also uploaded as ESI, show the transient traversal of the components in the vapor mixture *along the length of the fixed* bed from the inlet (position = 0) to the exit (position = 1). The molar gas-phase concentrations (units mol per m^3) are shown on the y-axis. In all cases, we note that the more weakly adsorbed component is present in higher concentrations in the gas phase, and traverses more quickly from the inlet to the exit. The more strongly adsorbed component is present in lower concentrations in the gas phase, and traverse more slowly.

The more weakly adsorbed component “breaks” through earlier, and we have the familiar breakthrough characteristics, shown below for 1-propanol/2-propanol at total pressure of 20 kPa as shown in Figure 2b of the main paper (shown below).

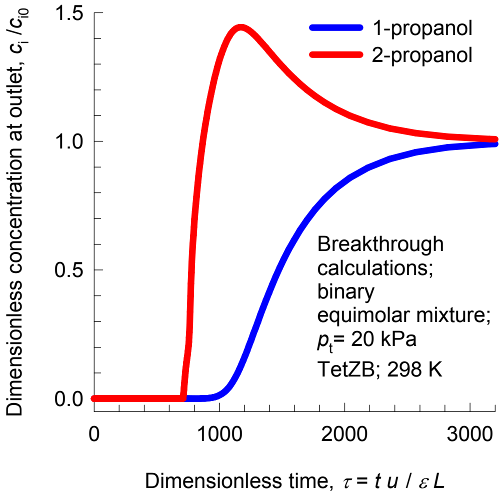

List of video animations attached:

Video S1. Video animations of separations of 1-/2-propanol mixture
Video S2. Video animations of separations of ethanol/1-propanol mixture
Video S3. Video animations of separations of ethanol/1-propanol mixture
Video S4. Video animations of separations of ethanol/benzene mixture
Video S5. Video animations of separations of ethanol/chloroform mixture
Video S6. Video animations of separations of acetone/methanol mixture
Video S7. Video animations of separations of acetone/chloroform mixture

Section S8: Notation

b_A	dual-Langmuir-Freundlich constant for species *i* at adsorption site A, $\mathrm{Pa}^{-\nu_i}$
b_B	dual-Langmuir-Freundlich constant for species *i* at adsorption site B, $\mathrm{Pa}^{-\nu_i}$
c_i	molar concentration of species *i* in gas mixture, mol m^{-3}
c_{i0}	molar concentration of species *i* in gas mixture at inlet to adsorber, mol m^{-3}
$Đ_i$	Maxwell-Stefan diffusivity, m^2 s^{-1}
L	length of packed bed adsorber, m
n	number of species in the mixture, dimensionless
N_i	molar flux of species *i*, mol m^{-2} s^{-1}
p_i	partial pressure of species *i* in mixture, Pa

p_t	total system pressure, Pa
q_i	component molar loading of species *i*, mol kg^{-1}
r_c	radius of crystallite, m
R	gas constant, 8.314 J mol^{-1} K^{-1}
t	time, s
T	absolute temperature, K
u	superficial gas velocity in packed bed, m s^{-1}
v	interstitial gas velocity in packed bed, m s^{-1}

Greek letters

ε	voidage of packed bed, dimensionless
Θ_i	loading of species *i*, molecules per unit cell
ρ	framework density, kg m^{-3}
τ	time, dimensionless

Subscripts

i	referring to component *i*
t	referring to total mixture

Section S9: References

1. P. K. Thallapally, J. Tian, M. R. Kishan, C. A. Fernandez, S. J. Dalgarno, P. B. McGrail, J. E. Warren and J. L. Atwood, *J Am Chem Soc*, 2008, **130**, 16842-+.
2. M. Sadakiyo, T. Yamada and H. Kitagawa, *J Am Chem Soc*, 2011, **133**, 11050-11053.
3. (a) R. Krishna and J. M. van Baten, *Langmuir*, 2010, **26**, 3981-3992; (b) R. Krishna and J. M. van Baten, *Langmuir*, 2010, **26**, 8450-8463; (c) R. Krishna and J. M. van Baten, *Langmuir*, 2010, **26**, 10854-10867; (d) R. Krishna and J. M. van Baten, *J. Membr. Sci.*, 2010, **360**, 476-482.
4. (a) E. D. Bloch, W. L. Queen, R. Krishna, J. M. Zadrozny, C. M. Brown and J. R. Long, *Science*, 2012, **335**, 1606-1610; (b) Z. R. Herm, B. M. Wiers, J. M. Van Baten, M. R. Hudson, P. Zajdel, C. M. Brown, N. Maschiocchi, R. Krishna and J. R. Long, *Science*, 2013, **340**, 960-964; (c) C. Gücüyener, J. van den Bergh, J. Gascon and F. Kapteijn, *J. Am. Chem. Soc.*, 2010, **132**, 17704-17706; (d) J. Yang, R. Krishna, J. Li and J. Li, *Microporous Mesoporous Mater.*, 2014, **184**, 21-27; (e) R. Krishna, *Micropor Mesopor Mat*, 2014, **185**, 30-50.
5. R. Krishna and J. R. Long, *J. Phys. Chem. C*, 2011, **115**, 12941-12950.
6. R. Krishna and R. Baur, *Sep. Purif. Technol.*, 2003, **33**, 213-254.
7. A. L. Myers and J. M. Prausnitz, *A.I.Ch.E.J.*, 1965, **11**, 121-130.